Evaluation of diffusion length and surface-recombination velocity from a planar-collector-geometry electron-beam-induced current scan

Evaluation of diffusion length and surface-recombination velocity from a planar-collector-geometry electron-beam-induced current scan

H. K. Kuiken and C. van Opdorp
Philips Research Laboratories, P. O. Box 80.000, 5600 JA Eindhoven, The Netherlands

(Received 19 July 1984; accepted for publication 25 October 1984)

For performing electron-beam-induced current (EBIC) measurements on sufficiently large samples, the use of a "planar-collector geometry" (i.e., with the collector covering part of the irradiated surface itself) is very attractive. However, the pertinent theoretical EBIC curves for finite surface-recombination velocities s have so far been lacking. This paper presents the complete theoretical expressions for arbitrary values of s and diffusion length L. Simple asymptotic solutions are given for point- and finite-size generation sources. Easy methods are developed to facilitate the application of these solutions in the practical evaluation of L and s from experimental EBIC curves. These methods are applied to experimental data available through the literature.

I. INTRODUCTION

A well-established method for measuring the minority-carrier diffusion length L of semiconductor materials makes use of the SEM-EBIC technique, see Refs. 1–3 and references therein. Using a scanning electron microscope (SEM), one generates excess charge carriers inside a sample by an incident high-energy electron beam. The generated minority carriers are collected by a Schottky or p-n diode made on or in the sample; this yields the electron-beam-induced current (EBIC). Variation of the position of beam incidence with respect to that of the collecting junction produces variation of the stationary EBIC value. Comparison of an experimental EBIC curve resulting from such a scan with theoretical curves permits evaluation of L.

Obviously the shape of an EBIC curve will depend not only on the value of L, but also on a number of geometrical and other factors. These are the shape and dimensions of the sample, the shape and position of the collecting junction and scanning track, and generation parameters. Apart from L there is still another material parameter with unknown value which greatly influences the shape of the curve, viz. the surface-recombination velocity s of the surface on which the beam is incident.

Generally the influence of s is considered as an annoying circumstance for accurate determination of L. From our point of view, on the contrary, its strong influence on the shape of the curve is advantageous in that it may enable one to evaluate not only L but also s from a given experimental EBIC scan. It is obvious that one of the prerequisites for this is a sufficiently accurate knowledge of the theoretical curves for the relevant geometry at different values of L and s.

In this paper we shall consider large samples whose dimensions amount to many diffusion lengths in all directions. The conventional geometry used for such samples is the "normal-collector geometry" shown in Fig. 1(a); the plane of the collecting Schottky or p-n junction is perpendicular to the irradiated surface. The theoretical curves for different values of L, s, and "effective generation depth" h (for this parameter, see Sec. II C) are well known for this geometry.[4,5] Even so, these full curves are seldom if ever used to evaluate L (and s) from experimental data, e.g., by curve fitting. The much simpler approach of restricting the analysis to the EBIC scan interval at sufficiently large collector-beam distance is apparently preferred. Here, the reciprocal slope of a semilogarithmic plot of EBIC versus distance roughly equals L, to a certain extent independently of the values of s and h. Obviously the applicability of the latter, much simpler approach is liable to certain restrictions. In order to know these restrictions, i.e., to really know what is meant by the foregoing loosely used expressions "sufficiently large distances," "roughly equals L," and "to a certain extent independently of s and h," it is still necessary to know the complete theoretical expressions for all distances and all values of s and h. Indeed their knowledge is even quite indispensable if one also wants to evaluate s from an experimental curve.

In an alternative large-sample geometry the collecting junction lies in the plane of the irradiated surface itself: part of the surface is covered by a Schottky or a very shallow p-n junction.[6] This is the "planar-collector geometry." We shall consider the case of the collector having a straight edge perpendicular to the scanning track, and normal beam incidence, as sketched in Fig. 1(b).

The planar-collector geometry has practical advantages over the normal geometry. For the latter, the required

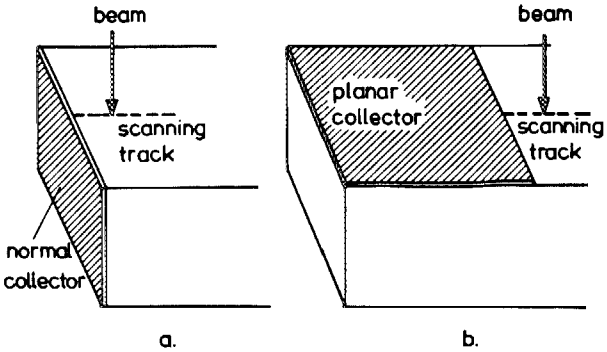

FIG. 1. Two basic geometrical configurations for performing EBIC measurements on large samples: (a) normal-collector geometry; junction perpendicular to irradiated surface, (b) planar-collector geometry; junction in plane of irradiated surface (or alternatively a very shallow p-n junction).

 0021-8979/85/062077-14$02.40

well-controlled cleaving of the sample frequently meets with problems. Another advantage of the planar-collector geometry is that it can also be used in the study of defects.[7] (Defect measurements are also performed with the electron beam incident normally to the collecting junction.) On the other hand, the calculation of theoretical curves is much more complicated for the planar than for the normal collector. For that reason the latter has been preferred in the past by most investigators.

Planar-collector analysis was already undertaken in Ref. 6. However, the authors calculated only the theoretical EBIC curves for the relatively simple case of $s = \infty$. Complete theoretical curves for finite s values have so far been lacking in the literature. Nevertheless, knowledge of these curves is indispensable for the same reasons as those mentioned above for the normal collector. In this paper we present the complete expressions for the theoretical EBIC curves for all possible values of L, s, and h for the planar collector.

The organization of the paper is as follows. Section II presents the mathematics which yield the theoretical expressions. In Sec. III we develop simple, fast procedures for applying these expressions in the evaluation of L and s from a given experimental EBIC curve. Practical examples of such evaluations are presented in Sec. IV. Section V gives the summary and conclusions.

II. MATHEMATICS

We assume here homogeneous and excitation-density-independent values of s and of the minority-carrier diffusion coefficient D and lifetime τ (and consequently also of $L = \sqrt{D\tau}$). Geometry and coordinates are depicted in Fig. 2. First we shall consider the solution due to a point source, subsequently that due to a source of finite size.

Those readers who are mainly interested in the application of the mathematical results might skip this section and continue with Sec. III.

A. Point source; general solution

The continuity equation for the excess minority-carrier density in the steady state Δn is given by

$$D \operatorname{div} \operatorname{grad}(\Delta n) - \Delta n/\tau = 0 . \tag{1}$$

The condition at the source can be written as

$$\lim_{r\to 0}\left(-4\pi r^2 D \frac{\partial(\Delta n)}{\partial r}\right) = G , \tag{2}$$

where G is the generation rate and r measures the distance from the source. We are interested only in the current through the collecting junction, which is given by

$$I = -qD\int_{-\infty}^{\infty} dz \int_{-\infty}^{0} dx \left(\frac{\partial(\Delta n)}{\partial y}\right)_{y=0} , \tag{3}$$

where q is the electronic charge. It has been shown in Refs. 4,8 that for this restricted purpose it is permissible to replace the point source by a homogeneous equivalent line source of equal strength per unit length:

$$\lim_{r\to 0}\left(-2\pi r D \frac{\partial(\Delta n)}{\partial r}\right) = G_l . \tag{4}$$

[G and G_l have the same nominal value, but dimensions of reciprocal time and reciprocal (time$\times$length), respectively.] In this paper we shall restrict ourselves to this two-dimensional carrier distribution.

The continuity equation can now be written as

$$\left(\frac{\partial^2}{\partial x^2} + \frac{\partial^2}{\partial y^2} - \frac{1}{L^2}\right)\Delta n = 0 , \tag{5}$$

where $L = \sqrt{D\tau}$. The boundary conditions are

$$y = 0 \begin{cases} x > 0: \ D\partial(\Delta n)/\partial y = s\Delta n , & (6) \\ x < 0: \ \Delta n = 0 , & (7) \end{cases}$$

and

$$\Delta n = 0 \quad \text{when} \quad r = [(x - x_s)^2 + (y - y_s)^2]^{1/2} \to \infty , \tag{8}$$

where (x_s, y_s) represents the line-source position. Only the case $x_s > 0$ will be considered.

To obtain a mathematical formulation with the smallest number of parameters it will be necessary to employ dimensionless variables. Let us introduce therefore

$$X \equiv x/L , \quad Y \equiv y/L , \quad R \equiv r/L , \tag{9}$$

$$\Delta N \equiv \Delta n D/G_l , \tag{10}$$

$$S \equiv sL/D . \tag{11}$$

The resulting problem definition depends now upon a single parameter only, which is S:

$$\left(\frac{\partial^2}{\partial X^2} + \frac{\partial^2}{\partial Y^2} - 1\right)\Delta N = 0 , \tag{12}$$

$$Y = 0 \begin{cases} X > 0: \ \partial(\Delta N)/\partial Y = S\Delta N , & (13) \\ X < 0: \ \Delta N = 0 , & (14) \end{cases}$$

$$\Delta N = 0 \quad \text{when} \quad R \to \infty , \tag{15}$$

and

$$\lim_{R\to 0}\left(-2\pi R \frac{\partial(\Delta N)}{\partial R}\right) = 1 . \tag{16}$$

Although this problem resembles in many respects that of the normal-collector geometry considered and solved by Van Roosbroeck[4] as far back as 1955, an analytical treatment of it is far more complicated. The fundamental difficulty is caused by the fact that this is a so-called mixed-boundary-value problem, in the sense that different boundary conditions apply at different parts of the single boundary $Y = 0$ [see Eqs. (13) and (14)]. It is not possible now to use the device employed by Van Roosbroeck involving image sources to represent the boundary conditions. To solve the present problem we must resort to a more powerful kind of method, which in our case comes down to the appli-

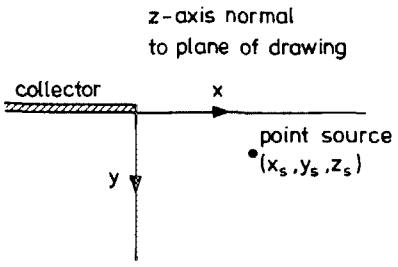

FIG. 2. Planar-collector geometry with indication of symbols. The z axis is perpendicular to the plane of drawing.

cation of the Wiener–Hopf technique.[9] Since the details involved in the application of this technique are rather complicated and lengthy, we have decided to present these elsewhere,[10] so that we may concentrate on the results here.

If we denote the electric current per unit length through the collecting junction by I_l, we have $I_l = -qD \times \int_{-\infty}^{0} [\partial(\Delta n)/\partial y]_{y=0} dx$. Upon the introduction of the dimensionless variable $Q \equiv I_l/qG_l = I/qG$, this reads

$$Q \equiv \frac{I}{qG} = -\int_{-\infty}^{0} \left(\frac{\partial(\Delta N)}{\partial Y}\right)_{Y=0} dX . \tag{17}$$

Here I is identical with the EBIC. The normalized EBIC, Q, is clearly the fraction of generated minority carriers that flows into the collecting junction. In Ref. 10 it has been derived that Q can be expressed as follows:

$$Q \equiv \frac{I}{qG} = \frac{(S+1)^{1/2}}{\pi} \int_1^{\infty} \frac{(1+\alpha)^{1/2}}{\alpha} e^{F(\alpha,S) - X_s\alpha} \times \frac{S \sin(Y_s\sqrt{\alpha^2-1}) + \sqrt{\alpha^2-1}\cos(Y_s\sqrt{\alpha^2-1})}{S^2+\alpha^2-1} d\alpha , \tag{18}$$

where

$$F(\alpha,S) = \frac{\alpha}{\pi} \int_0^{\pi/2} \frac{\ln(1+S\sin\theta)}{1+(\alpha^2-1)\sin^2\theta} d\theta . \tag{19}$$

For $S = 0$ a simpler expression can be obtained[10]:

$$Q = \tfrac{1}{2} e^{-Y_s} \operatorname{erfc}\{[(X_s^2+Y_s^2)^{1/2} - Y_s]^{1/2}\} + \tfrac{1}{2} e^{Y_s} \operatorname{erfc}\{[(X_s^2+Y_s^2)^{1/2} + Y_s]^{1/2}\} . \tag{20}$$

For $Y_s = 0$ this reduces further to

$$Q = \operatorname{erfc}(X_s^{1/2}) . \tag{21}$$

In Fig. 3 we present curves of $\ln Q$ vs X_s for different S values, as calculated with Eqs. (18) and (19), for a point source situated at the surface ($Y_s = 0$).

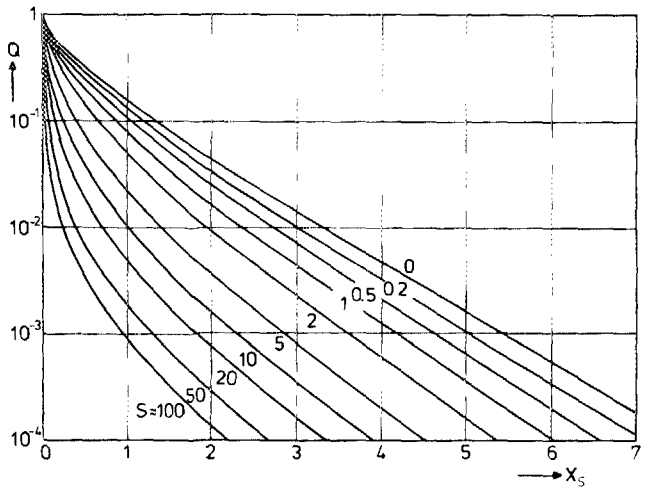

FIG. 3. Normalized semilogarithmic EBIC vs X_s curves for different values of the normalized surface-recombination velocity S as calculated from Eq. (18) with Eq. (19), for $Y_s = 0$ (point source situated at the surface).

B. Point source; asymptotic solution

The solution for the current as defined by Eqs. (18) and (19) can be used for numerical calculation, but it is rather too unwieldy for quick reference purposes. Very often an asymptotic solution which is valid when the generation point is more than a few diffusion lengths away from the edge of the junction is found to be most useful. At the cost of some effort we may derive such an asymptotic solution from Eqs. (18) and (19). The method we shall use is a kind of modified method of Laplace, which is explained in Appendix A. Like the classical method of Laplace[11] it makes use of the fact that, when $X_s \gg 1$, the main contribution to the integral of Eq. (18) comes from the immediate neighborhood of the lower bound $\alpha = 1$; an allowance is made here, however, for the circumstance that apart from the exponential the other parts of the integrand may also vary quite rapidly. This extra feature turns out to be particularly useful when X_s is indeed larger, but not very much larger than unity, e.g., for $X_s = 2$.

Applying the method put forward in Appendix A we find

$$Q \equiv \frac{I}{qG} \sim \frac{(1/S + Y_s) f(S) e^{-X_s}}{\left[X_s + g(S) + Y_s^2\left(\dfrac{1+SY_s/3}{1+SY_s}\right)\right]^{3/2}}, \quad (X_s \gtrsim 2), \tag{22}$$

where

$$f(S) = \frac{(S+1)^{1/2}}{\pi^{1/2} S} \exp\left[\frac{1}{\pi}\int_0^{\pi/2} \ln(1+S\sin\theta) d\theta\right], \tag{23}$$

and

$$g(S) = \frac{3}{4} + \frac{1}{\pi S} + \frac{3}{2S^2} - \frac{\sigma(S)}{\pi S^2} . \tag{24}$$

The function $\sigma(S)$ is given by Eqs. (A15) and (A16) of Appendix A. The functions $f(S)$ and $g(S)$ are shown in Fig. 4. For $S \to \infty$ they approach the asymptotes $f(S) \sim (2\pi)^{-1/2}$ and $g(S) \sim 3/4$.

When $Y_s \lesssim 1/3$, Eq. (22) becomes

$$Q \equiv \frac{I}{qG} \sim \frac{(1/S + Y_s) f(S) e^{-X_s}}{[X_s + g(S)]^{3/2}} . \tag{25}$$

To get an idea of the accuracy of the asymptotic solution as given by Eq. (22) one may consult Table I, which shows the amount by which Eq. (22) underestimates the true value given by Eq. (18) (Y_s has been taken equal to zero). It appears that the best approximations are obtained when S is about 2. When S increases beyond that value, the underestimation becomes greater; this seems to level off, however, so that it never becomes worse than a given limiting value. An accuracy of around 5% at source positions which are four diffusion lengths away from the collector seems quite acceptable. An accuracy of 13% at two diffusion lengths is quite close to the 14% level of the asymptotic solution for the normal collector, found in Ref. 5.

It is noteworthy that close to $S = 0$ the current is governed by a rule fundamentally different from that applicable in the $S \gg 1$ region. This can be seen by comparing the asymptotics of Eqs. (22) and (20). From Eq. (22) with Fig. 4 for $f(S)$ and $g(S)$ it follows that for $S \gg 1$ and larger X_s values, Q varies roughly as $e^{-X_s} X_s^{-3/2}$. As a matter of fact, it is shown by Eq.

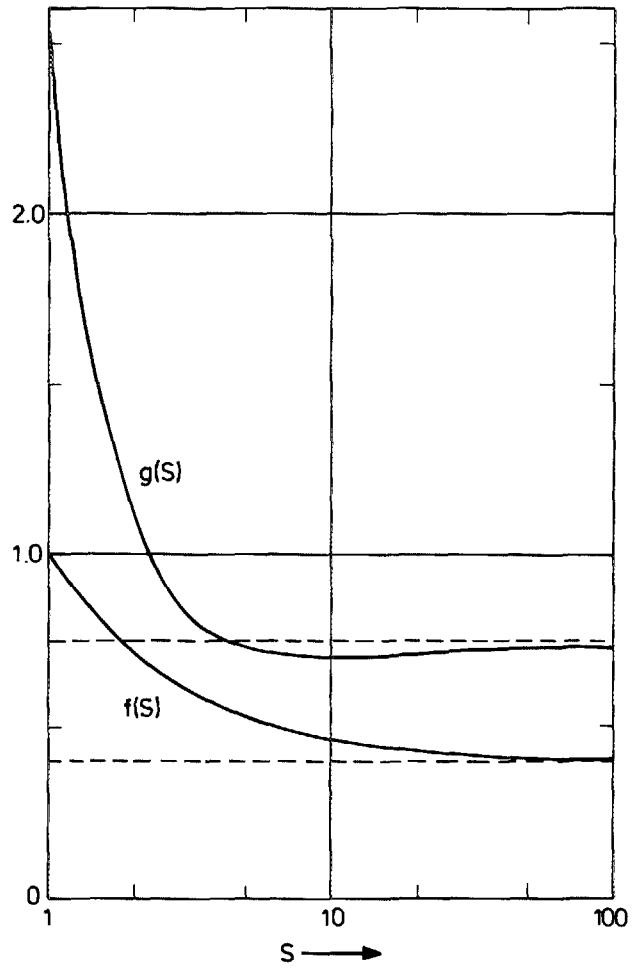

FIG. 4. The functions $f(S)$ and $g(S)$ figuring in the asymptotic expression for the EBIC of Eq. (22), for $S>1$. $f(S)$ and $g(S)$ were calculated from Eqs. (23) and (24) with Eq. (A15).

(6.15) of Ref. 10 that the asymptotics of Eqs. (22) and (25) are valid as long as $SX_s^{1/2} \gg 1$, provided that $X_s \gg 1$. This shows that these formulae may even be used when S is very small, but then only for exceedingly large values of X_s. On the other hand, when $SX_s^{1/2} \ll 1$, with $X_s \gg 1$, the relevant asymptotics follow directly from Eq. (20):

$$Q \sim \frac{e^{-X_s}}{(\pi X_s)^{1/2}} \left[1 - \frac{(Y_s^2+1)}{2X_s} + O\left(\frac{1}{X_s^2}\right) \right]; \tag{26}$$

thus Q varies here roughly as $e^{-X_s} X_s^{-1/2}$. These behaviors were noticed first in Ref. 12 for the limiting cases $S=\infty$ and $S=0$. However, whereas the authors presented the relevant analysis for $S=\infty$,[6] they did not show explicitly how their correct result for $S=0$ was obtained.

Further, when $SX_s^{1/2}$ is neither small nor large, the asymptotic behavior for $X_s \gg 1$ is rather complicated, as may be seen from Eq. (6.15) of Ref. 10. It is certainly quite different from the behavior surmized in Ref. 12, where it is assumed that Q varies roughly in proportion to $e^{-X_s} X_s^{-n}$ with $\frac{1}{2} < n < \frac{3}{2}$. In Appendix B we show that the asymptotic result obtained in Ref. 6 for $S=\infty$ agrees with our Eq. (22).

TABLE I. Underestimation of theoretical EBIC for given values of $S(=sL/D)$ and $X_s(=x_s/L)$, when using the asymptotic Eq. (22) instead of the exact Eq. (18).

	% underestimation	
S	$X_s=2$	$X_s=4$
1	19.4	9.8
2	7.3	3.0
5	10.5	4.3
10	12.4	4.9
100	13.0	5.0

C. Source of finite size; asymptotic solution for $S>1$

Although the foregoing results refer to point sources, it is possible to derive the solution for sources of nonvanishing size, on account of the linearity of the system of differential equation with boundary conditions, Eqs. (5)–(8). However, the complexity of Eq. (18) is considerable, so that it is not possible to derive useful analytical results on the basis of that equation. Of course, should it really be necessary, one may always use Eq. (18) to obtain a numerical solution pertinent to a special case.

If S is not too close to zero, the asymptotic solution of Eq. (22) would seem to be easier to deal with when sources of finite size have to be considered. If the source is much smaller than L, Eq. (25) applies for the contribution to Q from any point within the generation volume. The total current due to the generation distribution $\tilde{g}(X_s,Y_s,Z_s)$ is then given by

$$Q \equiv \frac{I}{qG} = f(S) \int_{\text{gen.vol.}} \left(\frac{1}{S} + Y_s\right) \frac{e^{-X_s}}{[X_s + g(S)]^{3/2}} \frac{\tilde{g}}{G} dV_s , \tag{27}$$

where

$$G = \int_{\text{gen.vol.}} \tilde{g} dV_s . \tag{28}$$

As the diameter of the generation volume is much smaller than L, the value of X_s will be virtually constant in the integrand of Eq. (27). On the other hand, since the generation volume is very close to the surface, the relative variations of Y_s across it are not negligible. This is why Eq. (27) can be approximated by

$$Q \equiv \frac{I}{qG} = \frac{(1/S + H) f(S) e^{-X_s}}{[X_s + g(S)]^{3/2}} , \tag{29}$$

where

$$H = \int_{\text{gen.vol.}} Y_s \frac{\tilde{g}}{G} dV_s , \quad (\ll 1) . \tag{30}$$

Equation (29) for Q of the finite source is identical with that for the point source, Eq. (25), except for the quantity H replacing the normalized point-source depth Y_s. Therefore H, the normalized "effective generation depth" of the finite source volume, can be considered as the depth of an equivalent point source. It can easily be shown that H equals Y_s^0 when the generation volume is a sphere with its center at (X_s^0, Y_s^0, Z_s^0), a radius that is not larger than Y_s^0 and a density distribution that is symmetrical with respect to the center. From the definition for H of Eq. (30), which was put forward

first in Ref. 5, the corresponding dimensional effective generation depth is given by

$$h = HL = \int_{\text{gen.vol.}} y_s \frac{\tilde{g}}{G}\, dV_s \,. \tag{31}$$

It is instructive to compare Eq. (29) with that for a point source at the surface. In the latter case one has from Eq. (22) with $Y_s = 0$:

$$Q \equiv \frac{I}{qG} \sim \frac{f(S)e^{-X_s}}{S\,[X_s + g(S)]^{3/2}} \,. \tag{32}$$

This equation is identical with that for a finite but not too large source, Eq. (29), apart from the factor $(1/S + H)$ in the latter replacing $1/S$ in the former. This substitution entails an enhancement by a factor $1 + SH = 1 + sh/D$ owing to the effective generation depth h of the finite source being finite rather than zero. In Appendix D we present a perspicuous physical interpretation of this enhancement factor in terms of an increased "surface-recombination resistance."

III. METHODS TO EVALUATE L AND S

Though the theoretical EBIC curves are now known from Eqs. (18) and (19) (cf. Fig. 3), their practical application in evaluating L and S from experimental EBIC curves may present problems. (Actually, an analogous situation occurs for the normal-collector geometry; this case was treated more briefly in Ref. 8.) In this section we present two straightforward methods for this purpose. An important characteristic of our approach is that it also estimates the *accuracy* of the values obtained for L and S. In Sec. IV we demonstrate the practicability of our methods by applying them to actual experimental data.

The first step of both methods is based on the asymptotic expression of Eq. (29), valid at $X_s \gtrsim 2$ and $S \gg 1$ for a finite-size source at a normalized effective depth $H = h/L \ll 1$ below the surface. [For the special case $H \ll 1/S$ or $h \ll D/s$ this equation simplifies to Eq. (32): a point source situated at the surface.] At sufficiently large X_s the term $g(S)$ in the denominator will become negligible. In that case Eq. (29) can be written as

$$Q\left(\frac{x_s}{L}\right)^{3/2} \approx \left(\frac{1}{S} + H\right) f(S) e^{-x_s/L} \,. \tag{33}$$

With $Q \equiv I/qG$, a good approximation L^* of the actual L then follows directly from the slope of a $\ln(Ix_s^{3/2})$ vs x_s plot:

$$\frac{1}{L^*} \equiv -\frac{d}{dx_s} \ln(Ix_s^{3/2}) \,. \tag{34}$$

To give an impression of the shapes expected, in Fig. 5(a) we have replotted the curves of Fig. 3 in a semilogarithmic $QX_s^{3/2}$ vs X_s plot (solid curves). The most conspicuous feature of these curves as compared to those of Fig. 3 is their typical domed structure. The distance of the current maximum from the junction edge, X_{top}, increases with decreasing S. In Fig. 5(b) we have plotted this X_{top} vs S relation; for not too high S values it is useful for obtaining a quick estimate of S.

The condition $X_s \gg g(S)$ is easier fulfilled for higher S values, cf. Fig. 4. In fact, Eq. (34) was already used in Refs. 6, 12, and 13, where it was assumed that $S \gg 1$; there was no

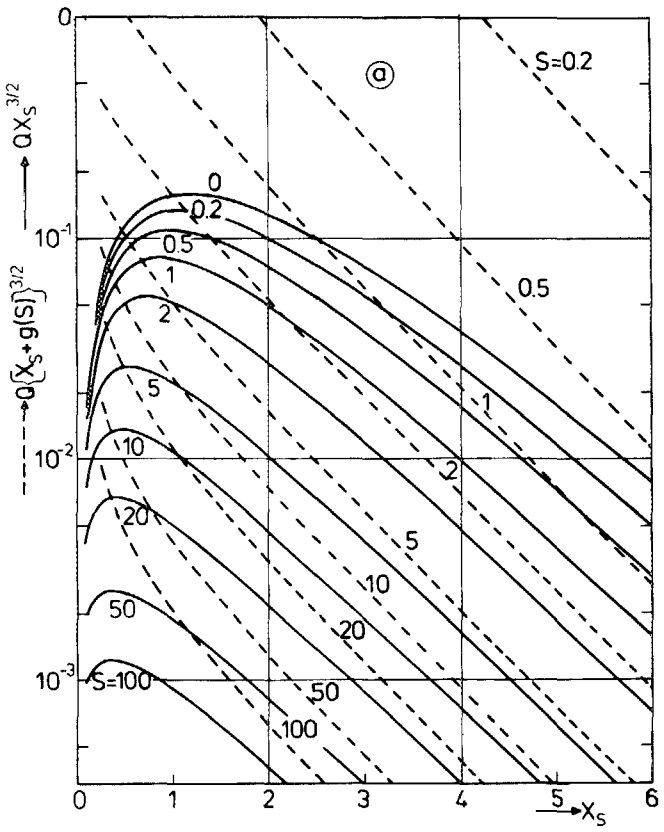

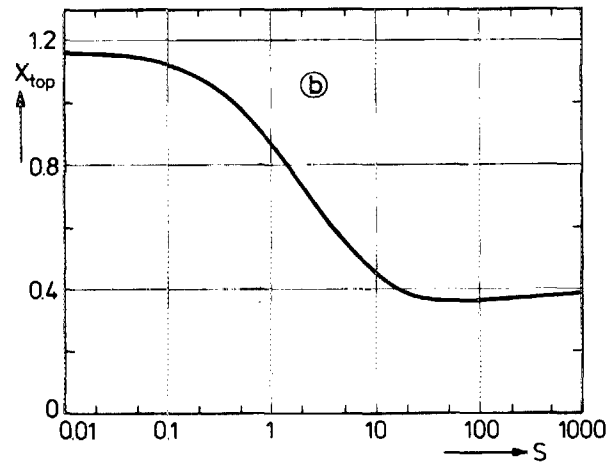

FIG. 5. (a) The theoretical EBIC curves of Fig. 3 in semilogarithmic $QX_s^{3/2}$ vs X_s plots (solid curves) and semilogarithmic $Q\,[X_s + g(S)]^{3/2}$ vs X_s plots (dashed curves). (b) Location of the top of the semilogarithmic $QX_s^{3/2}$ vs X_s plot [see Fig. 5(a)] as a function of S.

check on this condition being fulfilled. In Secs. III A and III B Eq. (34) will be used for a first estimate of L for arbitrary values of S; suitable iteration methods are shown to produce much better approximations.

A. The tangent-and-intersect method

We start by determining L^* according to Eq. (34) by drawing a tangent to the experimental curve at some point x_s in the tail of the curve plotted in a $\ln(Ix_s^{3/2})$ vs x_s diagram. Using this L^* we can find a better approximation. This is done by improving the approximation to the denominator of

Eq. (29) as compared to the first attempt, which yielded Eq. (33). Instead, we take now

$$Q\left(\frac{x_s}{L^*}+\frac{3}{4}\right)^{3/2}\approx\left(\frac{1}{S}+H\right)f(S)e^{-x_s/L}. \tag{35}$$

Here, since $g(S)$ is still unknown, we have tentatively substituted the value 3/4, valid for $S\gg 1$ (see Fig. 4). This yields the second approximation:

$$\begin{aligned}\frac{1}{L^{**}}&\equiv -\frac{d}{dx_s}\ln\left[I\left(\frac{x_s}{L^*}+\frac{3}{4}\right)^{3/2}\right]\\ &= -\frac{d}{dx_s}\ln(Ix_s^{3/2})-\frac{3}{2}\frac{d}{dx_s}\ln\left(\frac{\frac{x_s}{L^*}+\frac{3}{4}}{x_s}\right)\\ &=\frac{1}{L^*}+\frac{9}{8}\frac{1}{x_s\left(\frac{x_s}{L^*}+\frac{3}{4}\right)}.\end{aligned} \tag{36}$$

This equation directly yields L^{**} in terms of L^* and x_s.

What is the accuracy of the approximations L^* and L^{**} to the actual L? This question can be answered as follows. Choose one of the curves of Fig. 3 and consider this as a quasi-experimental curve. This means that along the horizontal axis values of the dimensional quantity x_s are given; the values of L and S are considered as unknown and have to be recovered from the curve.

Proceeding along the lines sketched above one finds in this case the ratios L^*/L and L^{**}/L of the approximate and actual diffusion lengths. Doing so for curves corresponding to different values of S, these ratios can be plotted vs ln S. This is done in Fig. 6. The values of L^*/L were calculated from tangents to the solid curves of Fig. 5(a) (and intermediate ones), drawn at distances X_s which amount to factors of 3, 5, or 8 times the corresponding current-maximum position X_{top}. It is seen that for decreasing X_s/X_{top} ratio or S value the accuracy decreases.

It turns out that the mean value

$$\hat{L}=\tfrac{1}{2}(L^*+L^{**}) \tag{37}$$

yields a much better approximation than both L^* and L^{**}. For not too low S values and $X_s/X_{top}\geq 3$ the error in $\hat{L}$ remains easily within a few percentage points. This serendipitous result is also presented in Fig. 6.

In the meantime, however, the value of S is still unknown. Even if one is not primarily interested in this quantity, a rough knowledge of its value is indispensable for estimating the error in $\hat{L}$ from Fig. 6.

From close inspection of Fig. 3 one can verify that the tangent drawn at $X_s=0.9$ to any given EBIC curve (for not too small S values) intersects the vertical axis at a factor $1/S$ below the peak of the current. Therefore, by drawing the tangent to an experimental EBIC curve at $x_s=0.9L\approx 0.9\hat{L}$, one finds an approximate value for S, provided the "ideal peak height" is known. The ideal peak height, i.e., the peak height that would result from using an ideal point source, will be higher than that obtained when using a realistic source of finite size. In Appendix C a way is treated to find the ideal peak height.

The value of the normalized surface recombination velocity obtained with the intersect method will be designated by S^*. This value suffices for consulting Fig. 6 in order to estimate the error made in L. An approximate value s^* of the dimensional surface-recombination velocity follows from an application of the definition $S=sL/D$, yielding $s^*=S^*D/\hat{L}$. The inherent error made in this way can be calculated as follows.

From the last two equations it follows that $s^*/s=(S^*/S)(L/\hat{L})$. This equation allows us to express the ratio s^*/s as a function of S using any of the Figs. 6(a), 6(b), or 6(c) for $\hat{L}/L$ vs S, together with Fig. 3 which provides us with the value of S^* for a given S, using the intersect method. The result is presented in Fig. 7. The three different curves resulting from using Fig. 6(a), 6(b), or 6(c) for $\hat{L}/L$ coincide, except

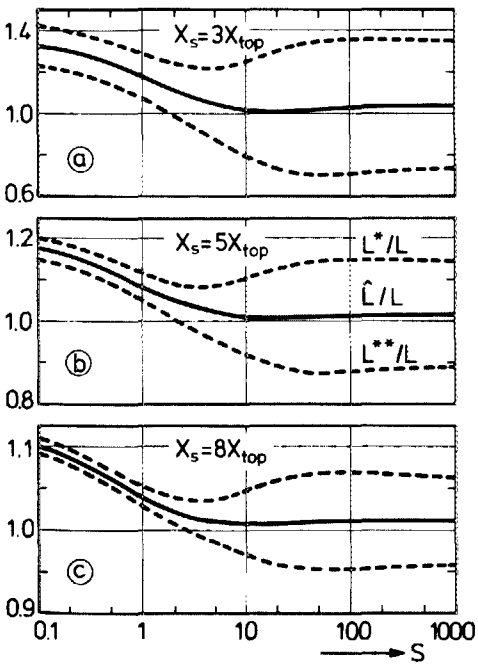

FIG. 6. The error in the diffusion length when evaluated with the tangent method [see Eqs. (34), (36), and (37)] as a function of S. The tangents were drawn at distances X_s of 3, 5, and 8 times the corresponding current-maximum position X_{top}, respectively. (Note the different vertical scales.)

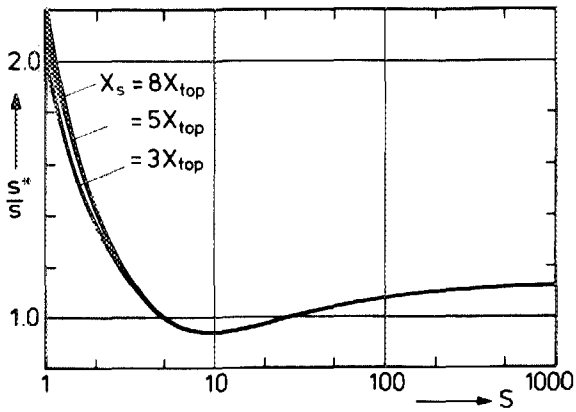

FIG. 7. The error in the dimensional surface recombination velocity $[s^*/s=(S^*/S)(L/\hat{L})]$ when evaluated with the intersect method of Sec. III A, as a function of the actual value of S. The three curves correspond with the three tangent positions of Fig. 6, used for determining $\hat{L}$.

at low S values. We conclude that the intersect method will yield fairly accurate results for $S \gtrsim 3$. When using Fig. 7, one employs the value of S^* for reading the horizontal axis.

The above intersect method for determining S was based on the curves of Fig. 3, which were calculated from Eq. (18) with Eq. (19), with $Y_s = 0$; in practice this requires $H \ll 1/S$ or $h \ll D/s$ (see introduction of Sec. III). This condition may be checked with the aid of the relation

$$h = AV_0^{1.75}, \tag{38}$$

where V_0 is the acceleration voltage for the incident electrons.[14] The quantity A is a known constant for a given semiconductor material,[1,14] e.g., for Si one has $A = 3.84 \times 10^{-12}$ cm/V$^{1.75}$ (Ref. 5).

Let us consider now the case that the condition $h \ll D/s$ is *not* fulfilled. Comparison of the asymptotics of Eqs. (29) and (32) shows that in the higher X_s-region the finite-source curve is identical with the point-source curve, apart from a parallel vertical shift. Assuming that this is already roughly the case at $X_s = 0.9$, the tangent at this point will intersect the vertical axis approximately at $1/S + H$ rather than at $1/S$ below the peak. Using Eq. (38) this allows rough calculation of S. Another suggestion is to reduce V_0 so much that the point-source condition $s \ll D/h$ does become fulfilled.

We want to note here that Eq. (38) also suggests quite a different way of determining S. Rather than measuring the variation of the EBIC with varying x_s, one now keeps x_s constant and varies the effective depth h of the source by varying V_0. The generation rate will also vary, viz. according to

$$G = BI_0V_0. \tag{39}$$

Here I_0 is the current of the incident high-energy electrons, and B is a constant for a given semiconductor material, cf. Eq. (A22); the value is irrelevant here. Substitution of Eqs. (38) and (39) in Eq. (29) yields

$$Q \equiv \frac{I}{qG} = \frac{I}{qBI_0V_0} = C\left(\frac{1}{S} + \frac{AV_0^{1.75}}{L}\right). \tag{40}$$

For fixed values of X_s and S, the quantity C is constant. From Eq. (40) it follows that by plotting $I/(I_0V_0)$ vs $V_0^{1.75}$ one may expect a straight line. The slope of this line and its intercept with the ordinate axis are given by $slope = qABC/L$ and $intercept = qBC/S$. Therefore s follows from

$$s = \frac{SD}{L} = \frac{D}{A}\frac{\text{slope}}{\text{intercept}}. \tag{41}$$

B. Tail-fitting method

An important difference between the first and the present method concerns the way of evaluating S. The intersect method basically made use of the fact that for not too low S values the asymptotes of the curves of Fig. 3 are depressed by a factor of roughly $1/S$ [or $(1/S + H)$ for a finite-size source] with respect to the ideal peak height. For the present method no knowledge of the ideal peak height is needed: rather than using the dependence of the *level* of the asymptotes with respect to the peak, it makes use of the dependence of the *shape* of the measured interval on the value of S. This is done by the application of a curve-fitting procedure involving the tail of the curve. From Eq. (29) it appears that as far as the asymptotic region is concerned, the latter dependence originates from the function $g(S)$ in the denominator. From Fig. 4 it appears that the influence of S is strong for S values near unity. Indeed, it will turn out that the present method yields optimum results in this region; in a sense it can be considered as complementary to the intersect method, which works better for higher S values.

The initial step of the present method resembles that of the first method in that $g(S)$ is tentatively taken zero, cf. Eq. (33). In the next steps, increasingly better values of $g(S)$ are used.

To show how this method works, we shall simulate a set of results that might be the outcome of a typical experiment. Let us assume quite arbitrarily that $L = 1.85\,\mu$m and $S = 1$. The corresponding values of $Q \equiv I/qG$ may be calculated from Eq. (18) for a series of values of the dimensional dis-

TABLE II. Tail-fitting applied to "experimental" values for $S = 1$ and $L = 1.85$.

x_s	I	$\ln(Ix_s^{3/2})$	$X_s = x_s/L$	$\ln[I(X_s + 0.726)^{3/2}]$	$X_s = x_s/L$	$\ln[I(X_s + 1.37)^{3/2}]$	$X_s = x_s/L$
1.5	0.11144		0.679		0.761		0.798
2	0.07029		0.905		1.015		1.064
2.5	0.04561		1.131		1.269		1.330
3	0.03020		1.358		1.523		1.569
3.5	0.02030		1.584		1.777		1.862
4	0.01381		1.810		2.031		2.128
4.5	0.00949	−2.401	2.036	−3.134	2.284	−2.713	2.394
5	0.00657	−2.611	2.262	−3.383	2.538	−2.980	2.660
5.5	0.00458	−2.829	2.489	−3.635	2.792	−3.246	2.926
6	0.00321	−3.054	2.715	−3.888	3.046	−3.513	3.192
6.5	0.00226	−3.285	2.941	−4.143	3.300	−3.780	3.457
7	0.00160	−3.519	3.167	−4.399	3.553	−4.046	3.723
7.5	0.00114	−3.754	3.394	−4.653	3.807	−4.310	3.989
	L	2.21		1.97		1.88	
	I_1/I_3		28.1		21.3		19.4
	S		5.25		1.60		1.2
	$g(S)$		0.726		1.37		

tance x_s. Again, the purpose of the method is to recover the values of L and S from these simulated results.

The method is illustrated by Table II, which shows three iteration steps; this leads to $L = 1.88\ \mu$m, which is close to the exact value. In each step the tail of the current profile is used to estimate L by means of a least-squares fit (straight line). As we have found, it is not advisable to carry out too many iteration steps, the reason being that the procedure does not seem to converge. We recommend that the procedure be limited to three steps. In that case one will always achieve an improvement upon the result of the initial step.

For obtaining increasingly better estimates of S we made use of Fig. 8(a), which presents the ratio I_1/I_3 as a function of S. Here I_1 denotes the current at $X_s = 1$ and I_3 the current at $X_s = 3$. The curves of Fig. 8(a) and (b) show that such ratios may be good indicators of the value of S as long as S is of order unity. Far from unity the ratio method is no longer feasible, since the ratio of currents is then virtually independent of S. On the other hand, this phenomenon offers the possibility of determining the diffusion length L in yet another way. If one knows beforehand that $S \geqslant 10$, one might find two positions of the electron beam in such a way that I_1/I_3 is in the range 29.5–30. The first position is then just one diffusion length away from the contact edge. This method is very sensitive since in the large-S range one has $I_{0.9}/I_{2.7} \sim 23.8$ and $I_{1.1}/I_{3.3} \sim 36.3$. If the range covered by a given experiment is shorter than three diffusion lengths, the method of Fig. 8(a) cannot be applied. For this reason we present Fig. 8(b) which refers to narrower ranges.

To show how the tail-fitting works out in the lower and the larger S ranges, we present Table III for $L = 1.85\ \mu$m and $S = 0.1$, and Table IV for $L = 1.85\ \mu$m and $S = 10$. (Just as for the first method, the relative accuracy for the present method is independent of the particular choice of L.) In the lower S range the method is still seen to be quite adequate as far as the determination of L is concerned. The error is about 3%. The predicted value of S only gives an indication of its range. For large values of S the present method is somewhat less accurate, but, as far as L is concerned, the error remains under 10%. Nothing can be said about the exact value of S, except that it is large. In analogy with the tangent method (cf. Fig. 6), the present method could be improved considerably, particularly for large S, if the least-squares fit would be carried out for much smaller values of the current that are obtained at larger generation distances. In Table IV we restricted ourselves to the lower end of the third decade. Since for large S the decay of the current is rather fast when the point of generation is moved away from the junction, the third decade refers to generations at only a few diffusion lengths away from the junction edge. In that case the asymptotic formula (29) is valid only approximately. Alternatively, when S is very large, the method based on Fig. 8 may be used with more success. In that case a range of only three diffusion lengths is sufficient.

Note that for a finite-size source the procedures of this section yield directly the value of S itself, whereas the intersect method of Sec. III A generally yields the value of $(1/S + H)^{-1}$.

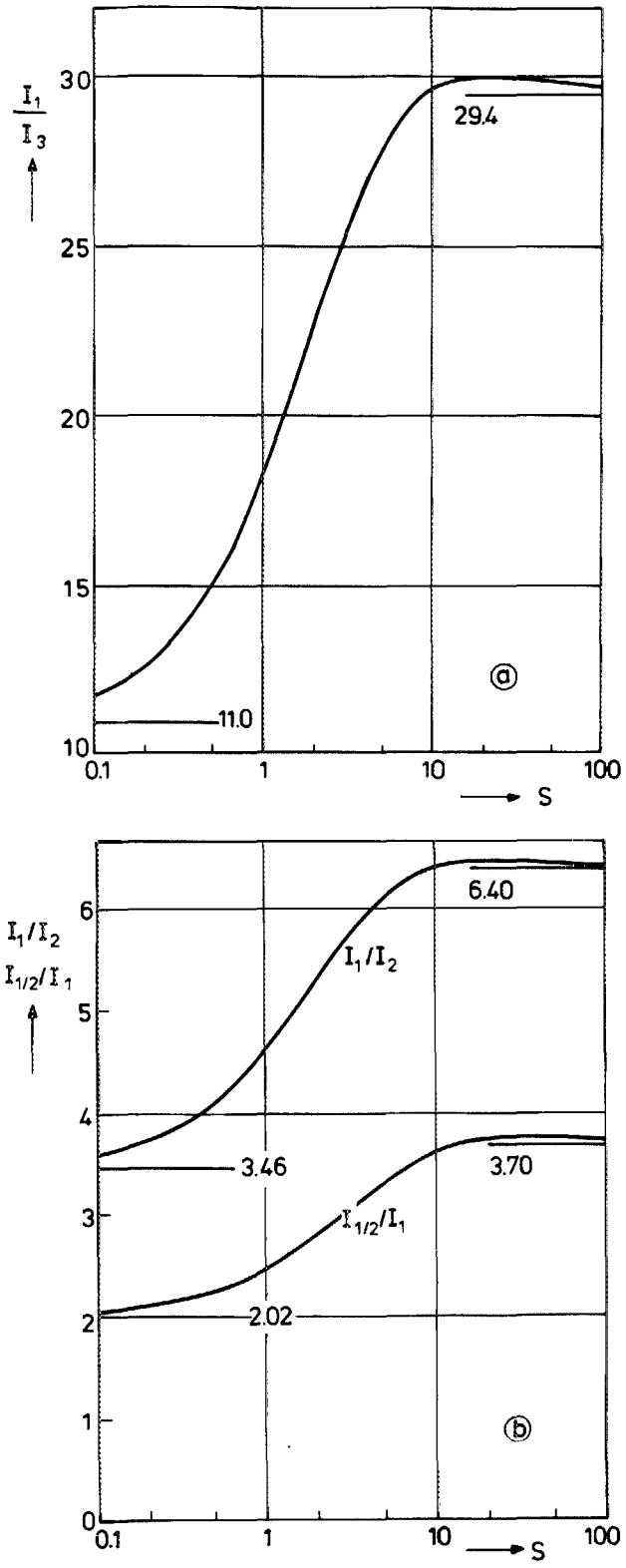

FIG. 8. (a) Ratio of the EBIC values at distances of one and three diffusion lengths from the collecting junction edge, as a function of S. (b) The same for the ratios at distances of one and two, and at distances of a half and one diffusion length, respectively.

C. Summary of methods

The results of this section may be summarized as follows. Two methods were developed for the evaluation of L: the tangent method [Eq. (37) with Eqs. (34) and (36)] and the improved tail-fitting method [based on a stepwise improve-

TABLE III. Tail-fitting applied to "experimental" values for $S = 0.1$ and $L = 1.85$.

x_s	I	$\ln(Ix_s^{3/2})$	$X_s = x_s/L$	$\ln[I(X_s + 1.228)^{3/2}]$	$X_s = x_s/L$	$\ln[I(X_s + 4.878)^{3/2}]$	$X_s = x_s/L$
1.5	0.18844		0.625		0.704		0.789
2	0.12961		0.833		0.939		1.053
2.5	0.09067		1.042		1.174		1.316
3	0.06419		1.250		1.409		1.579
3.5	0.04583		1.458		1.643		1.842
4	0.03295		1.667		1.878		2.105
4.5	0.02381		1.875		2.113		2.368
5	0.01729		2.083		2.347		2.632
5.5	0.01260		2.292		2.582		2.895
6	0.00921	−2.000	2.500	−2.714	2.817	−1.627	3.158
6.5	0.00675	−2.191	2.708	−2.943	3.052	−1.892	3.421
7	0.00496	−2.388	2.917	−3.174	3.286	−2.157	3.684
7.5	0.00365	−2.591	3.125	−3.407	3.521	−2.421	3.947
8	0.00269	−2.799	3.333	−3.642	3.756	−2.685	4.211
8.5	0.00199	−3.010	3.542	−3.876	3.991	−2.946	4.474
9	0.00147	−3.227	3.750	−4.115	4.225	−3.210	4.737
9.5	0.00109	−3.445	3.958	−4.353	4.460	−3.471	5.000
10	0.00081	−3.665	4.167	−4.590	4.695	−3.730	5.263
	L	2.40		2.13		1.90	
	I_1/I_3		22.1		16.3		12.8
	S		1.78		0.68		0.21
	$g(S)$		1.228		4.878		

ment of S in Eq. (32)]. For evaluating S, three methods are at our disposal: that of the tangent intersecting the ordinate, the X_{top} method [Fig. 5(b)], and the current-ratio method (Fig. 8).

These methods for evaluating L and S were presented here in the special arrangements of Secs. III A and III B. Put together as such, the methods are complementary in different S intervals with regard to the optimum accuracies that can be attained for both L and S. Roughly speaking, the method of Sec. III A is accurate when $S \gtrsim 3$, whereas that of Sec. III B yields good results when $S \lesssim 5$. However, should we leave optimum-accuracy considerations for what they are, we could combine any of the methods for evaluating S with either method for L. For instance, the *easiest* way to evaluate L is to invoke the tangent method, whereas S is readily obtained by the current-ratio method. Moreover, in the specific interval $3 \lesssim S \lesssim 5$ the corresponding accuracies are high for *both*.

To complete this summary two further methods should be mentioned: the voltage-varying method for determining S [Eq. (41)], and the asymptotic current-ratio method to evaluate L when $S \gtrsim 10$, as suggested in Sec. III B.

TABLE IV. Tail-fitting applied to "experimental" values for $S = 10$ and $L = 1.85$.

x_s	I	$\ln(Ix_s^{3/2})$	$X_s = x_s/L$	$\ln[I(X_s + 0.75)^{3/2}]$	$X_s = x_s/L$	$\ln[I(X_s + 0.813)^{3/2}]$	$X_s = x_s/L$
1.5	0.01639		0.745		0.904		0.888
1.75	0.01195		0.845		1.054		1.036
2.00	0.00890		0.966		1.205		1.183
2.25	0.00674		1.087		1.355		1.331
2.50	0.00518		1.208		1.506		1.479
2.75	0.00402		1.329		1.657		1.627
3.00	0.00315	−4.112	1.449	−4.587	1.807	−4.316	1.775
3.25	0.00249	−4.228	1.570	−4.742	1.958	−4.467	1.923
3.50	0.00198	−4.346	1.691	−4.895	2.108	−4.617	2.071
3.75	0.00158	−4.468	1.812	−5.047	2.259	−4.767	2.219
4.00	0.00127	−4.589	1.932	−5.196	2.410	−4.914	2.367
4.25	0.00103	−4.708	2.053	−5.339	2.560	−5.054	2.515
4.50	0.00083	−4.838	2.174	−5.492	2.711	−5.205	2.663
	L	2.07		1.66		1.69	
	I_1/I_2		7.28		5.81		5.93
	S		large		3.3		3.64
	$g(S)$		0.75		0.813		

IV. APPLICATION TO EXPERIMENTAL DATA

The object of this section is to demonstrate the application of the evaluation techniques of the preceding section to available experimental data. Published data for the planar-collector geometry are scarce and exclusively bear upon Si material.

A. Experiments by Ioannou and Davidson[13]

In a paper by Ioannou and Davidson[13] $\ln(Ix_s^{3/2})$ vs x_s plots are presented for planar-collector-geometry EBIC experiments on boron-implanted and annealed p-type silicon. We shall focus our attention on the upper curve of Fig. 2(b) of their paper, i.e., the one from which the authors of Ref. 13 derived a diffusion length of 42 μm assuming $S=\infty$. It is seen that the curve exhibits the typical domed structure that we encountered in the curves presented in Fig. 5(a).

First of all we remark that the maximum of the curve is to be found just below 40 μm. With a diffusion length of 42 μm we have $X_s = x_s/L \approx 1$ at this maximum. Consulting Fig. 5(b) we see that the value of $S = sL/D$ must be smaller than unity in this case. Since for these lower values of S the first method of Sec. III does not lead to accurate results, we applied tail fitting. To be able to do this we measured the coordinates of the experimental points of Fig. 2(b) of Ref. 13 as accurately as possible. The results are shown in Table V.

Comparing Table V with either Table II, III, or IV, we see that the Tables V and III are similar in nature. Not only the general trends of the consecutive diffusion lengths and surface-recombination velocities are the same, even the relative sizes of the corrections are seen to be of the same orders of magnitude. On the basis of this we may conclude that L will be around 33.5 μm with S around 0.2. With $L = 33.5\,\mu$m, the maximum of the $\ln(Ix_s^{3/2})$ vs x_s curve is at $X_s \sim 1.1$–1.2, and this is seen to be in good agreement with our Fig. 5(b).

The value $S \approx 0.2$ corresponds with s between 60 and 600 cm/s. (The doping concentration being unknown, we took D between 1 and 10 cm^2/s.[15]) Though such low values are not uncommon in Si,[16–19] they are perhaps unexpected for the material under consideration.

The main conclusion of this subsection is that, by looking at the tail of the $\ln(Ix_s^{3/2})$ vs x_s plot, and trying to approximate this by a straight line as done in Ref. 13, one overestimates the diffusion length by about 25% when S is small. The simple tail-fitting procedure of Ref. 13 is practically identical with the initial step of our tangent method [Eq. (34)]. Indeed, consulting Fig. 6 we may predict an overestimation of the order found above. Our improved tail-fitting method yields values of L that are wrong by a few percentage points only, disregarding experimental inaccuracies. Of course, it is to be expected that both these error percentages could decrease when accurate tail sections are available for large values of x_s.

B. Experiments by Davidson and Dimitriades[12]

In Fig. 7 of Ref. 12 again $\ln(Ix_s^{3/2})$ vs x_s curves are presented for heat-treated Si; neither type nor doping concentration were given. These curves are somewhat different from those of Ref. 13 in that the curved sections are rather less conspicuous. The two middle curves show remnants of sections that do veer away from the straighter sections of the $\ln(Ix_s^{3/2})$ vs x_s plots. In the two other plots the curved sections are totally absent.

Referring now to the two middle curves we are led to

TABLE V. Tail-fitting applied to the upper curve of Fig. 2(b) of Ref. 13 (I is known, up to a multiplicative constant).

x_s	$Ix_s^{3/2}$	I	$\ln(Ix_s^{3/2})$	$X_s = x_s/L$	$\ln[I(X_s + 0.935)^{3/2}]$	$X_s = x_s/L$	$\ln[I(X_s + 3.05)^{3/2}]$	$X_s = x_s/L$
9.5	27.81	0.9498		0.222		0.249		0.275
19.3	35.25	0.4157		0.452		0.507		0.559
28.4	40.00	0.2643		0.665		0.745		0.823
37.9	41.28	0.1769		0.888		0.995		1.099
47.7	40.00	0.1214		1.117		1.252		1.383
56.8	38.45	0.0898		1.330		1.491		1.646
66.3	35.53	0.0658		1.553		1.740		1.922
75.7	29.86	0.0453		1.773		1.987		2.194
85.2	23.94	0.0304		1.995		2.236		2.470
94.7	18.74	0.02034	2.9307	2.218	−2.173	2.486	−1.328	2.745
104.1	15.14	0.01425		2.438		2.732		3.017
113.6	12.43	0.01027	2.5201	2.660	−2.659	2.982	−1.883	3.293
123.1	9.96	0.00729		2.883		3.231		3.568
132.5	8.05	0.00528	2.0857	3.103	−3.150	3.478	−2.430	3.841
142.6	6.40	0.00376		3.340		3.743		4.133
151.5	4.85	0.00260	1.5790	3.548	−3.702	3.976	−3.028	4.391
161.3	4.05	0.00198		3.778		4.234		4.675
170.4	3.27	0.00147	1.1848	3.991	−4.131	4.472	−3.496	4.939
		L	42.7		38.1		34.5	
		I_1/I_3		24.3		17.7		14.1
		S		2.5		0.91		0.38
		$g(S)$		0.935		3.05		

believe that the maxima of the $\ln(Ix_s^{3/2})$ vs x_s curves are to be found around $x_s/L = X_s \approx 0.4$. Consulting our Fig. 5(b) we see that the samples used by the authors of Ref. 12 must have had S values much larger than unity, as they indeed assumed themselves. With $S \geqslant 10$, $D \approx 4\,\mathrm{cm}^2/\mathrm{s}$ (Ref. 18) and $L \approx 40\,\mu\mathrm{m}$ (average value for the curves considered, as reported in Ref. 12) one finds values of s larger than 10^4 cm/s. This is several orders of magnitude higher than the s-values found in Sec. IV A for the Si samples of Ref. 14. In view of literature data[16–19] the values found in the present case appear on the high side.

Since $S \geqslant 10$, the tangent-and-intersect method is preferable here. We shall apply this method to the second curve (as seen from the top) of Fig. 7 of Ref. 12, from which the authors found $L \approx L^* = 52\,\mu\mathrm{m}$ (in actual fact, by remeasuring the slope we found $L^* = 49.7\,\mu\mathrm{m}$).

In Ref. 12, the straight section of the curve will probably be representative of the tangent at a position somewhere half way down the line, i.e., around $x_s = 90\,\mu\mathrm{m}$. Using Eq. (36) with $L^* = 49.7\,\mu\mathrm{m}$ we find

$$\frac{1}{L^{**}} = \frac{1}{49.7} + \frac{9}{8}\frac{1}{90\left(\frac{90}{49.7} + 0.75\right)} = \frac{1}{40.0}\,\mu\mathrm{m}^{-1}. \quad (42)$$

This yields $\hat{L} = \frac{1}{2}(L^* + L^{**}) = 44.8\,\mu\mathrm{m}$. To evaluate S more accurately, the intersect method cannot be applied here, owing to a lack of knowledge concerning E_0 and I_0, which would be needed to evaluate the ideal peak height Eq. (A22).

As $S \geqslant 10$, an alternative way of evaluating L is provided by the asymptotic current-ratio method. Taking the said curve of Ref. 12, we may shift L in such a way that I_1/I_3 is in the range 29.5–30 [see Fig. 8(a)]. (To be able to carry out this procedure here, we approximated the I vs x_s profile by a quadratic spline based on a point-wise representation of the curve: parabolic approximations in each interval between two consecutive sample points; the slopes continuous at the interval boundaries.) This yielded $L = 44.7\,\mu\mathrm{m}$.

The overestimation of L by the simple tail-fitting method of Ref. 12 is only 13% here. Precisely as in the case of Sec. IV A, this is consistent with the prediction from Fig. 6: for $X_s = 5X_{\mathrm{top}}$ ($X_s = 90/45 = 2$ and $X_{\mathrm{top}} \approx 0.4$) and $S \geqslant 10$ one expects an overestimation somewhere between 10% and 14%.

V. SUMMARY AND CONCLUDING REMARKS

For performing EBIC measurements on a sufficiently large sample, the planar-collector geometry has practical advantages over the normal-collector geometry. For the planar collector the knowledge of theoretical EBIC curves, which is indispensable for the evaluation of L and S from experimental curves, has been lacking until now (except for $S = \infty$). We have derived the complete mathematical expressions for the EBIC taking arbitrary values of L and S for a point source situated at an arbitrary depth y_s below the surface [Eqs. (18) and (19)]. These expressions are unwieldy; for easier handling an asymptotic solution has been derived for $x_s \gtrsim 2L$ and $S \geqslant 1$, Eq. (22). For small enough source depth $y_s \ll D/s\,(< L)$ this solution reduces further to Eq. (32), the expression for a point source situated at the surface.

For a source of any finite size the general expression for the EBIC can in principle be obtained by spatial integration of Eq. (18). Under the realistic condition of small source dimensions compared to L, the asymptotic solution takes the simple shape of Eq. (29). This solution is identical with that for the point source at the surface, Eq. (32), apart from an enhancement factor $(1 + sh/D)$; here h represents the effective source depth, i.e., the weighted center of the finite-source volume.

For the evaluation of both L and S from a given experimental EBIC curve, simple methods have been developed. The application of these methods to experimental EBIC curves brings to light, among other things, that L can be severely overestimated when it is erroneously assumed that $S \geqslant 1$.

An interesting feature of EBIC curves in a $\ln(Ix_s^{3/2})$ vs x_s plot is the presence of a maximum whose position yields an indication of the value of S, see Figs. 5(a) and 5(b). Since these theoretical curves are convex for all values of S, experimental data which produce concave curves in such a plot, like those of Ref. 6, should be regarded with due reservation.

When applying our results one should keep in mind the assumption made in the first paragraph of Sec. II, viz. that of excitation-independent values of L and s. The experimental excitation density can be varied between certain limits, which may provide a check on this assumption. Another point is that one should be careful to choose the proper position for the current meter, in order to avoid the disturbing contribution of the specimen current to the EBIC. Since these problems are not specific to the planar-collector geometry, they were not pursued here. More attention to these points has been paid in Refs. 5 and 8, respectively.

APPENDIX A: DERIVATION OF THE ASYMPTOTIC FORMULA OF EQ. (22)

It can easily be seen from Eqs. (18) and (19) that the integrand of Eq. (18) is proportional to $(\alpha - 1)^{1/2}$ when α gets down to unity. Therefore, we shall write the integrand as follows

$$e^{-\alpha X_s}(\alpha - 1)^{1/2} M(\alpha - 1) \quad (A1)$$

near the lower bound $\alpha = 1$. Here M is a function that admits an ordinary Taylor series expansion around the value zero of its argument. Let us consider the asymptotic behavior of the integral

$$J(X_s) = \int_1^\infty e^{-\alpha X_s}(\alpha - 1)^{1/2} M(\alpha - 1)\,d\alpha, \quad (A2)$$

when $X_s \to \infty$, with the proviso that we wish to use the asymptotic result for values of X_s that are not exceedingly large, say $X_s = 2$ and up. In case the coefficients of the Taylor series expansion of M are not small, i.e., if M varies rather rapidly near $\alpha = 1$, the classical method of Laplace yields a result of limited usefulness. This is why we proceed as follows. Let us rewrite Eq. (A2):

$$J = e^{-X_s}\int_0^\infty e^{-tX_s} t^{1/2} M(t)\,dt$$
$$= \frac{2}{3} e^{-X_s} M(0) \int_0^\infty e^{-tX_s + \ln\left(\frac{M(t)}{M(0)}\right)}\, dt^{3/2}$$
$$= \frac{2}{3} e^{-X_s} M(0) \int_0^\infty e^{-X_s\sigma^{2/3} + \ln\left(\frac{M(\sigma^{2/3})}{M(0)}\right)}\, d\sigma\,. \tag{A3}$$

Now we change the integration variable in the following way

$$\gamma^{2/3} = X_s\sigma^{2/3} - \ln\left(\frac{M(\sigma^{2/3})}{M(0)}\right). \tag{A4}$$

In the classical method of Laplace the second term on the right would not have been included. Substituting Eq. (A4) into Eq. (A3) we obtain

$$J \sim \frac{2}{3} e^{-X_s} M(0) \int_0^\infty \frac{e^{-\gamma^{2/3}}}{\left(X_s - \frac{M'(\sigma^{2/3})}{M(\sigma^{2/3})}\right)\left[X_s - \sigma^{-2/3}\ln\left(\frac{M(\sigma^{2/3})}{M(0)}\right)\right]^{1/2}} d\gamma\,, \tag{A5}$$

where a prime denotes differentiation with respect to the argument. If now we perform a partial integration, i.e., by integrating the e power, we get

$$J \sim \tfrac{2}{3} e^{-X_s} M(0) \times \frac{\int_0^\infty e^{-\gamma^{2/3}} d\gamma}{\lim_{\sigma\to 0}\left(X_s - \frac{M'(\sigma^{2/3})}{M(\sigma^{2/3})}\right)\left[X_s - \sigma^{-2/3}\ln\left(\frac{M(\sigma^{2/3})}{M(0)}\right)\right]^{1/2}} + \text{higher-order terms}\,, \tag{A6}$$

which can be further reduced to

$$J \sim \frac{\Gamma(\frac{3}{2})}{\left(X_s - \frac{M'(0)}{M(0)}\right)^{3/2}} M(0) e^{-X_s} + \text{higher-order terms}\,. \tag{A7}$$

Here the higher-order terms tend to zero faster than the one retained, when $X_s \to \infty$. The prime denotes differentiation with respect to the argument.

This result will now be applied to Eq. (18). From the definition of the function M implied by Eq. (A2) we have

$$M(t) = \frac{(S+1)^{1/2}}{\pi}\frac{(t+2)^{1/2}}{t+1} e^{F(t+1,S)} \times \frac{S\frac{\sin\left[Y_s\sqrt{t(t+2)}\right]}{t^{1/2}} + \sqrt{t+2}\cos\left[Y_s\sqrt{t(t+2)}\right]}{S^2 + t(t+2)}, \tag{A8}$$

from which

$$M(0) = \frac{2}{\pi}\frac{(S+1)^{1/2}}{S}\left(Y_s + \frac{1}{S}\right) e^{F(1,S)}, \tag{A9}$$

where the function F is defined by Eq. (19). Since $\Gamma(3/2) = \pi^{1/2}/2$, the numerator of Eq. (22) follows easily from Eqs. (A7) and (A9).

To derive the denominator of Eq. (22) we have to determine $M'(0)$ which involves some cumbersome algebra. One may either apply the chain rule or a method involving a two-term Taylor-series expansion about $t = 0$. The result is

$$-\frac{M'(0)}{M(0)} = g(S) + Y_s^2\frac{1 + SY_s/3}{1 + SY_s}, \tag{A10}$$

where

$$g(S) = -F'(1,S) + \frac{1}{2} + \frac{2}{S^2}. \tag{A11}$$

Here the prime denotes differentiation with respect to the first argument of F. The derivative in the last equation may be calculated explicitly. We have from Eq. (19)

$$F'(1,S) = \frac{1}{\pi}\int_0^{\pi/2} \ln(1 + S\sin\theta)\cos 2\theta\, d\theta\,. \tag{A12}$$

By partial integration, followed by the substitution $\sin\theta = t$, this can be further reduced to

$$F'(1,S) = -\frac{S}{\pi}\int_0^1 \frac{t(1-t^2)^{1/2}}{1+St}\, dt\,. \tag{A13}$$

The integral in this equation is elementary and we find

$$F'(1,S) = -\frac{1}{4} + \frac{1}{2S^2} - \frac{1}{\pi S} + \frac{1}{\pi S^2}\sigma(S)\,, \tag{A14}$$

where

$$\sigma(S) = \sqrt{S^2-1}\,\ln(S + \sqrt{S^2-1}) \quad \text{when } S > 1 \tag{A15}$$

and

$$\sigma(S) = \sqrt{1-S^2}\left[\arcsin(S) - \frac{\pi}{2}\right] \quad \text{when } 0 < S < 1\,. \tag{A16}$$

APPENDIX B: A COMPARISON OF EQ. (22) WITH A KNOWN SOLUTION FOR $S = \infty$

In Ref. 6 an exact solution was derived for $S = \infty$. From Eqs. (13) and (14) we see that in this case the condition $\Delta N = 0$ prevails along the complete boundary $Y = 0$. It is now possible to obtain the solution by means of the method of images. The current can be expressed as follows[6]:

$$Q = \frac{Y_s}{\pi}\int_{-\infty}^0 \frac{K_1(U^{1/2})}{U^{1/2}}\, dX\,, \tag{A17}$$

where K_1 is a modified Bessel function and where

$$U = (X - X_s)^2 + Y_s^2\,. \tag{A18}$$

Using the two-term asymptotic expansion for K_1, valid for large values of the argument,[20] we obtain

$$Q \sim \frac{Y_s}{(2\pi)^{1/2}}\int_{-\infty}^0 e^{-U^{1/2}}\left(\frac{1}{U^{3/4}} + \frac{3}{8}\frac{1}{U^{5/4}} + \ldots\right) dX$$
$$\sim \frac{Y_s}{(2\pi)^{1/2}}\int_{-\infty}^0 e^{-(X_s - X)}\frac{1}{(X_s - X)^{3/2}} \times\left[1 + \left(\frac{3}{8} - \frac{1}{2}Y_s^2\right)\frac{1}{X_s - X} + O\left(\frac{1}{(X_s - X)^2}\right)\right]. \tag{A19}$$

By means of partial integration (the first term twice, the higher-order terms only once) we arrive at

$$Q \sim \frac{Y_s}{(2\pi)^{1/2}} e^{-X_s} \left[\frac{1}{X_s^{3/2}} - \left(\frac{9}{8} + \frac{1}{2} Y_s^2 \right) \frac{1}{X_s^{5/2}} + O\left(\frac{1}{X_s^{7/2}} \right) \right] . \tag{A20}$$

Returning now to our Eq. (22) taking the limit $S \to \infty$, we have

$$\begin{aligned} Q &\sim \frac{Y_s}{(2\pi)^{1/2}} e^{-X_s} \frac{1}{\left(X_s + \frac{3}{4} + \frac{Y_s^2}{3} \right)^{3/2}} \\ &= \frac{Y_s}{(2\pi)^{1/2}} e^{-X_s} \frac{1}{X_s^{3/2}} \frac{1}{\left[1 + \left(\frac{3}{4} + \frac{Y_s^2}{3} \right) \frac{1}{X_s} \right]^{3/2}} \\ &= \frac{Y_s}{(2\pi)^{1/2}} e^{-X_s} \frac{1}{X_s^{3/2}} \left[1 - \frac{3}{2} \left(\frac{3}{4} + \frac{Y_s^2}{3} \right) \frac{1}{X_s} + O\left(\frac{1}{X_s^2} \right) \right] \end{aligned} \tag{A21}$$

and this is seen to be equal to Eq. (A20) up to the same order of approximation. We emphasize that this approximation is also correct when Y_s is of the order of unity.

APPENDIX C: CALCULATION OF THE IDEAL EBIC PEAK HEIGHT

For the evaluation of S using the intercept method we need to know the absolute value of the ideal peak height of the EBIC. This is the peak height for the fictitious case of a point source situated at the surface having the same strength G as the actual finite source. For such a point source when situated at the collector edge $X_s = 0$, all excess minority carriers generated would be caught by the junction field. Thus we have to calculate the value of the generation rate G, which proceeds as follows.

Let the kinetic energy of the incident electrons be E_0, their current I_0, and the average energy needed for the generation of an electron-hole pair e_i. If all incident electrons were to dissipate their whole energy within the sample, the pair generation rate would amount to $(I_0/q)(E_0/e_i)$. However, a certain fraction f of the incident electrons is scattered back into vacuum after one or more elastic and nonelastic collisions, leaving the sample with an average kinetic energy kE_0. Taking this energy loss into account, the ideal peak height of the EBIC, qG, is given by

$$qG = (1 - fk) I_0 E_0 / e_i . \tag{A22}$$

The values of f,[21] k,[22] and e_i[23,24] can be found in the literature, while I_0 can simply be determined by using a Faraday cage.

APPENDIX D: SOURCE OF FINITE SIZE: THE ENHANCEMENT FACTOR $(1 + sh/D)$

From Eqs. (29) and (32), which are valid for $X_s \geqslant 2 \gg H$ and $S \geqslant 1$, it was seen that the expression for Q for the finite source is nearly identical to that for the point source at the surface. The only difference is that the former is enhanced with a factor $1 + SH \equiv 1 + sh/D$. This result from the complete mathematical treatment can also be arrived at in the following, less rigorous, but more perspicuous way.

Let us consider the maximum excess carrier concentration Δn_0 brought about by a source with a given generation rate G; the position of this maximum concentration coincides with that of the equivalent point source. The value attained for Δn_0 depends on the resistances of the channels through which the excess carriers can reach the three recombination or drain sites, viz. surface, junction and bulk. Under the mentioned conditions for x_s, h, and s, a large majority of the generated electrons recombine directly at the surface; only a small fraction recombines in the bulk and an even smaller fraction manages to reach the collecting junction, where it produces the EBIC. Since the "surface-recombination resistance" which the minority carriers meet before vanishing at the surface is the smallest of the three parallel resistances mentioned, it determines the value of Δn_0 practically all by itself. The reason why we are interested in the value of the "effective source strength" Δn_0 is that it represents the "driving potential" for the EBIC drain component.

For the restricted purpose of calculating Δn_0 we may replace the equivalent point source by a fictitious generation plane parallel to the surface at depth h; the justification for this runs along lines analogous to those presented in Ref. 8 (see p. 204). Now for the one-dimensional plane-source geometry, in view of $h \ll L$, the excess carrier concentration profile has the linear shape $\Delta n(y) = \Delta n_s + (\Delta n_0 - \Delta n_s) y/h$, where Δn_s represents the value of $\Delta n(y)$ at the surface itself. The associated diffusion flux equals $(D/h)(\Delta n_0 - \Delta n_s)$. As a consequence of our assumptions, minority-carrier-flux continuity requires near equality of the generation rate G, the mentioned diffusion flux, and the recombination rate at the surface: $G \approx (D/h)(\Delta n_0 - \Delta n_s) \approx s \Delta n_s$. This yields $\Delta n_0 \approx (1 + sh/D) \Delta n_s \approx (1 + sh/D) G/s$. For $h = 0$ this reduces to the trivial result $\Delta n_0 (h = 0) = \Delta n_s = G/s$. For a finite source with effective generation depth h, the "effective source strength" Δn_0 is enhanced by a factor $\Delta n_0 / \Delta n_s = 1 + sh/D$ with respect to that of the point source located at the surface. Due to the linearity of the problem, the EBIC will be enhanced by the same factor. From our approach it is seen that $(1 + sh/D)$ can be considered as the factor by which the "surface-recombination resistance" is enhanced due to the nonzero depth h.

[1] H. J. Leamy, J. Appl. Phys. **53**, R51 (1982).
[2] J. I. Hanoka and R. O. Bell, Ann. Rev. Mater. Sci. **11**, 353 (1981).
[3] A. Azim Khan and John A. Woollam, Appl. Phys. Commun. **2**, 17 (1982).
[4] W. Van Roosbroeck, J. Appl. Phys. **26**, 380 (1955).
[5] F. Berz and H. K. Kuiken, Solid-State Electron. **19**, 437 (1976).

[6]Dimitris E. Ioannou and Charalabos A. Dimitriadis, IEEE Trans. Electron Devices **ED-29,** 445 (1982).
[7]H. J. Leamy, L. C. Kimerling, and S. D. Ferris, Scanning Electron Microsc. **1,** Pt. IV, 529 (1976).
[8]C. van Opdorp, Philips Res. Rep. **32,** 192 (1977).
[9]B. Noble in *Methods Based on the Wiener–Hopf Technique for the Solution of Partial Differential Equations* (Pergamon, London, 1958).
[10]J. Boersma, J. J. E. Indenkleef, and H. K. Kuiken, J. Eng. Math. **18,** 315 (1984).
[11]C. M. Bender and S. A. Orszag, *Advanced Mathematical Methods for Scientists and Engineers* (McGraw–Hill, New York, 1978), Chap. 6.4.
[12]S. M. Davidson and C. A. Dimitriades, J. Microscopy **118,** 275 (1980).
[13]D. E. Ioannou and S. M. Davidson, J. Phys. D **12,** 1339 (1979).
[14]T. E. Everhart and P. H. Hoff, J. Appl. Phys. **42,** 5837 (1971).
[15]E. M. Conwell, Proc. IRE **46,** 1281 (1958).
[16]T. M. Buck and F. S. McKim, J. Electrochem. Soc. **105,** 709 (1958).
[17]A. Many, Y. Goldstein, and N. B. Grover, *Semiconductor Surfaces* (North-Holland, Amsterdam, 1965), p. 363.
[18]Andrew S. Grove, *Physics and Technology of Semiconductor Surfaces* (Wiley, New York, 1967), p. 145.
[19]R. L. Pritchard, *Electrical Characteristics of Transistors* (McGraw–Hill, New York, 1967), p. 71.
[20]M. Abramowitz and I. A. Stegun, *Handbook of Mathematical Functions* (Dover, New York, 1964), p. 378.
[21]H. E. Bishop, Br. J. Appl. Phys. **18,** 703 (1967).
[22]E. J. Sternglass, Phys. Rev. **95,** 345 (1954).
[23]F. S. Goulding and Y. Stone, Science **170,** 280 (1970).
[24]D. B. Holt, M. D. Muir, P. R. Grant, and I. M. Boswarva, *Quantitative Scanning Electron Microscopy* (Academic, London, 1974), p. 226.